Figures and figure supplements

The E3 ubiquitin ligase mindbomb1 controls planar cell polarity-dependent convergent extension movements during zebrafish gastrulation

Vishnu Muraleedharan Saraswathy *et al*

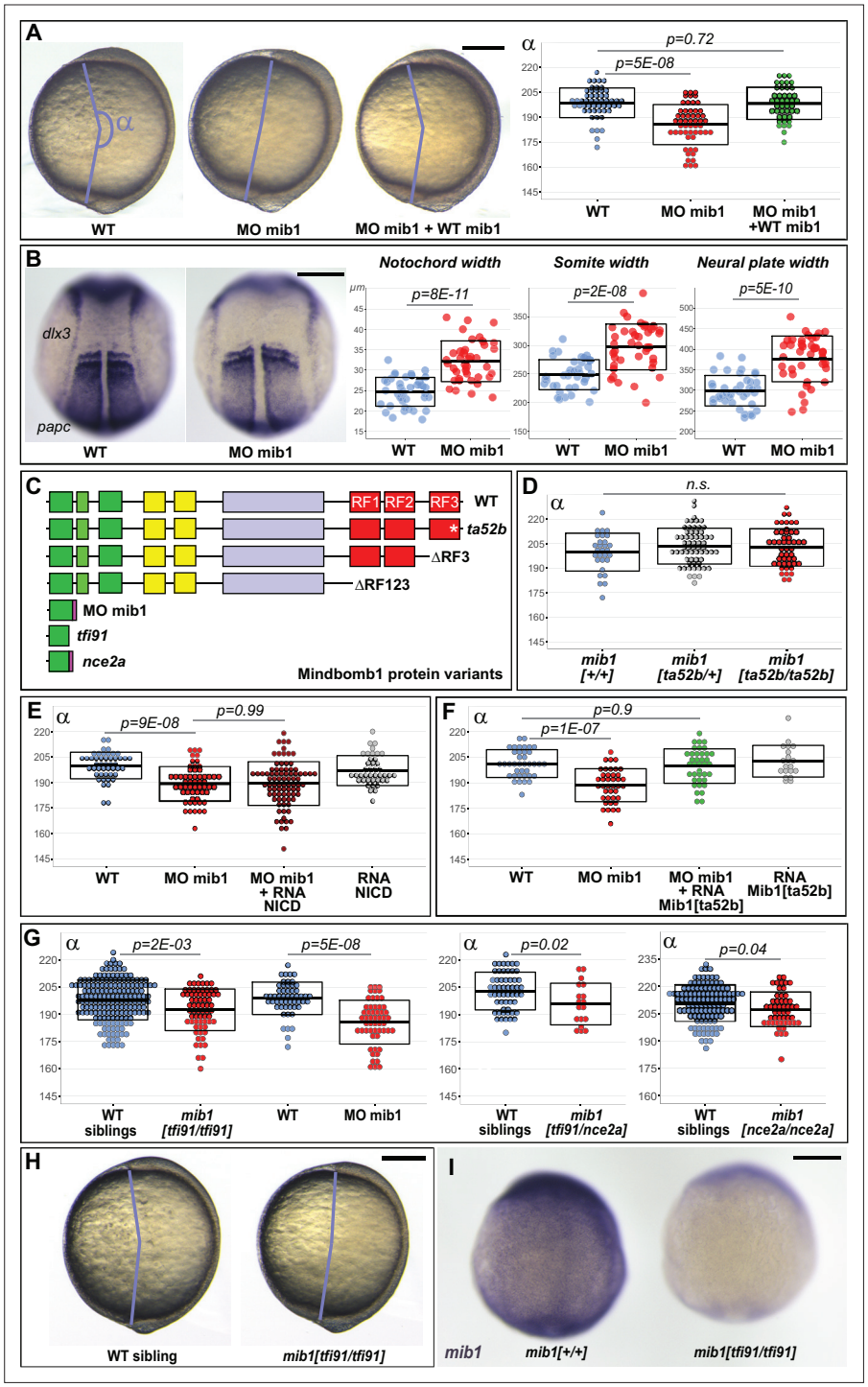

Figure 1. Mib1 regulates PCP-dependent convergent extension movements independently of Notch. (**A**) Axis extension was quantified at bud stage by measuring the axis extension angle α. Axis extension is reduced in mib1 morphants but restored upon coinjection of WT mib1 RNA. Lateral views of bud stage embryos, anterior up, dorsal to the right. (**B**) mib1 morphants present a widening of the notochord, somites, and neural plate. Dorsal views of 2 somite stage embryos, anterior up. *dlx3* in situ hybridization outlines the neural plate, *papc* the somites and the adaxial cells lining the notochord. Widths indicated in microns. (**C**) Mib1 protein variants used in the study. (**D**) The *mib1*^{ta52b} mutation has no effect on axis extension. (**E**) Constitutively activated Notch (NICD) fails to restore mib1 morphant axis extension. (**F**) mib1^{ta52b} RNA injection restores mib1 morphant axis extension. (**G,H**) Axis extension is impaired in *mib1*^{tfi91} or *mib1*^{nce2a} null mutants. On the left panel of (G) the mib1 morphant data from (**A**) are included for comparison. (**I**) In situ hybridization reveals reduced *mib1* transcript levels in n = 27 *mib1*^{tfi91} mutant

Figure 1 continued on next page

Figure 1 continued

embryos. Dorsal views of bud stage embryos, anterior up. To warrant identical acquisition conditions, two embryos were photographed on a single picture. Scalebars: 200 µm. Boxes in (**A,B, D–G**) represent mean values ± SD. See ***Figure 1—source data 1*** for complete statistical information.

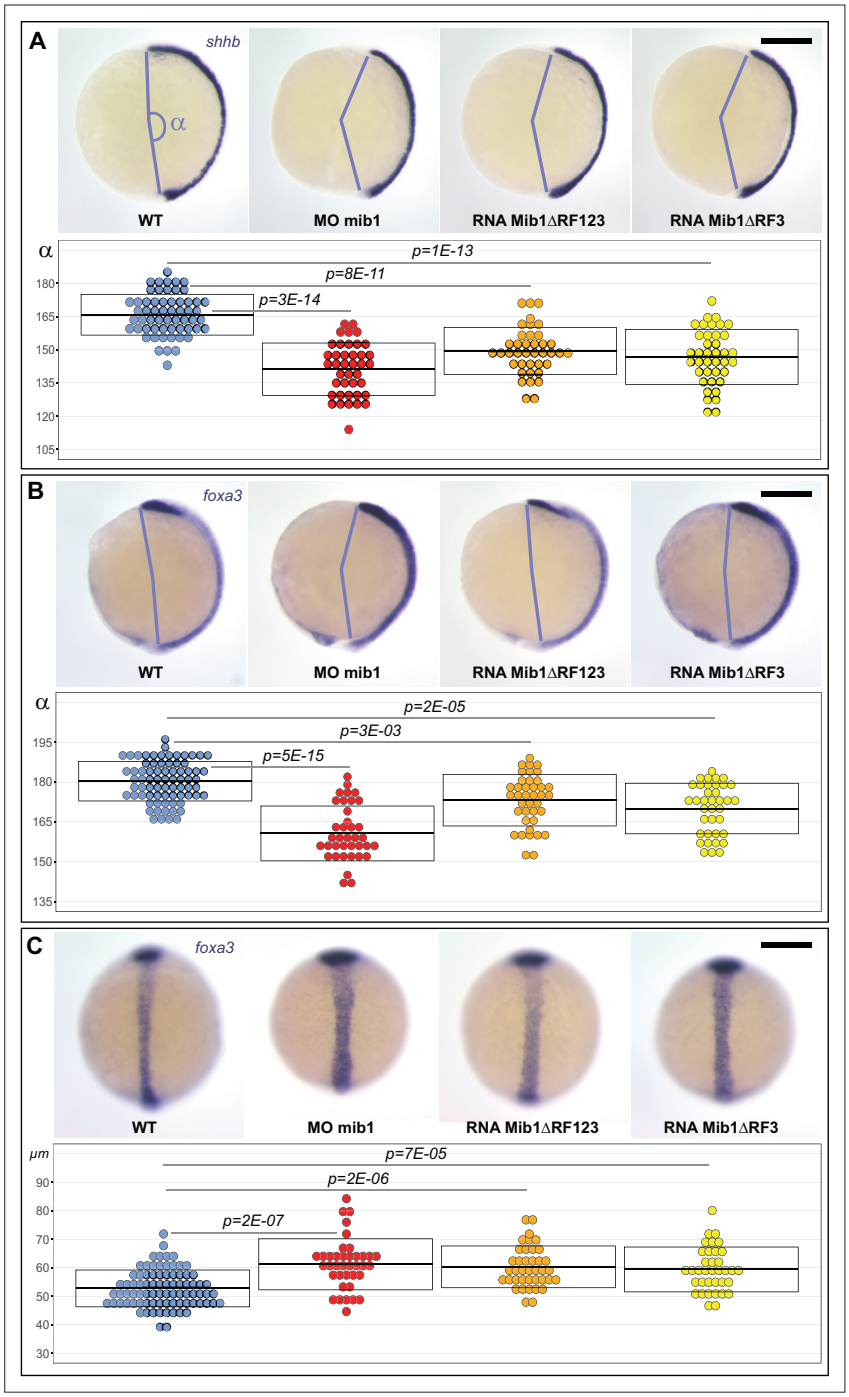

Figure 1—figure supplement 1. Mib1 knock-down impairs axial elongation. (**A,B**) Axis elongation was quantified at bud stage by measuring the axis extension angle α using the marker genes *shhb* (A, expressed in the notochord) and *foxa3* (B, expressed in notochord and prechordal plate). Axis extension is reduced following injection of mib1 morpholino (MO mib1) or RNAs encoding Mib1ΔRF123 or Mib1ΔRF3. Lateral views of bud stage embryos, anterior up, dorsal to the right. (**C**) Dorsal views of bud stage embryos stained for *foxa3* also reveal a significant widening of the Notochord. Boxes represent mean values ± SD. See ***Figure 1—source data 1*** for complete statistical information.

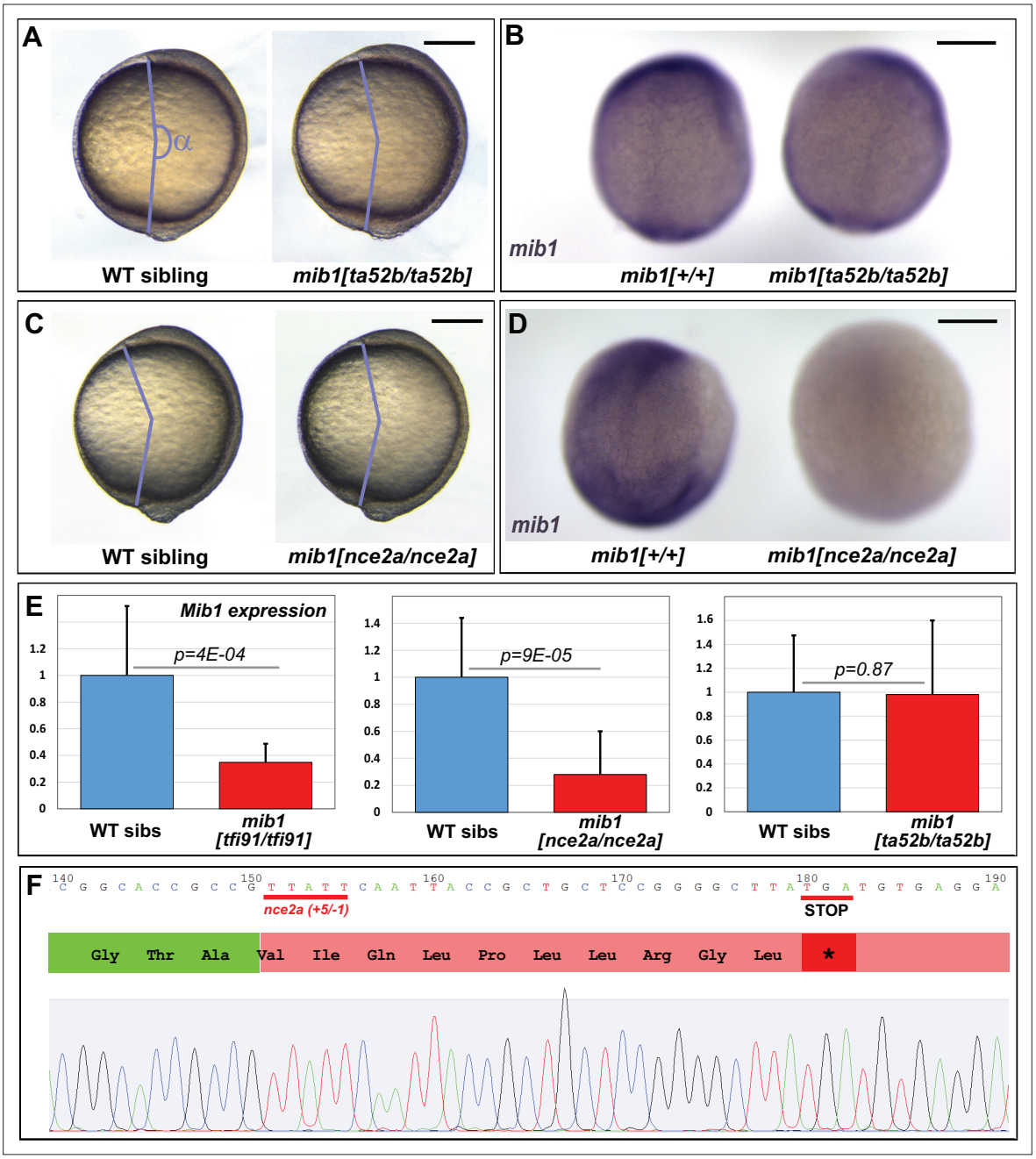

Figure 1—figure supplement 2. Axis extension and RNA expression in different *mib1* mutants. (**A,B**) Analysis of bud stage axis extension (**A**) and *mib1* in situ hybridization (**B**) show that the *mib1*^{ta52b} mutation does not impair Convergent Extension (CE) or *mib1* transcript abundance (B, n = 4 mutant embryos analyzed). (**C,D**) In contrast *mib1*^{nce2a} mutants present a weak reduction of CE (**C**) and a loss of *mib1* transcripts (D, n = 6 mutant embryos). (**E**) qPCR analysis of *mib1* transcript levels (30 hfp stage). *mib1*^{tfi91} and *mib1*^{nce2a} homozygous mutants present a reduction in *mib1* transcripts that is not observed for the *mib1*^{ta52b} allele. Error bars represent SE from three biological replicates. (**F**) *mib1*^{nce2a} mutants present a CrisprCas-induced InDel that causes a frame shift and leads to premature protein truncation. (**A,C**) depict lateral views of bud stage embryos, anterior up, dorsal to the right. A quantitative analysis of the corresponding data sets is provided in ***Figure 1D and G***. (**B,D**) Represent dorsal views of bud stage embryos, anterior up. To warrant identical acquisition conditions, two embryos were photographed on a single picture. Scalebars: 200 µm.

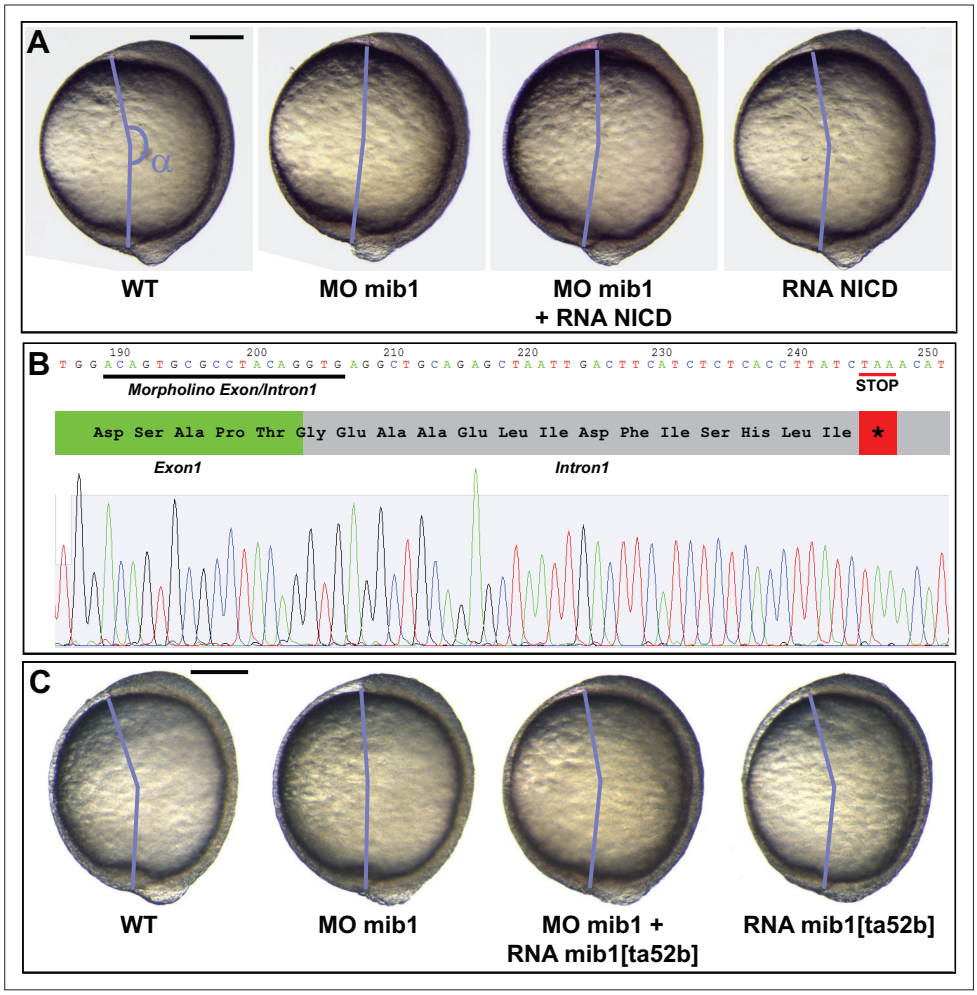

Figure 1—figure supplement 3. Mib1 regulates convergent extension independently of Notch. (**A**) Mib1 morphants display reduced convergent extension (quantified through the measure of the axis extension level α) that is not rescued by constitutively activated Notch (NICD). (**B**) cDNA sequence from wild-type embryos injected with mib1 exon/intron1 splice morpholino. Morpholino injection causes a retention of intron 1. As a consequence, the Mib1 morphant proteins comprises only the first 76 amino acids of WT Mib1 followed by 14 intronically encoded residues and a premature Stop codon. (**C**) Mib1 morphant axis extension can be restored through the overexpression of Notch-signaling-deficient mib1^{ta52b}. (**A,C**) depict lateral views of bud stage embryos, anterior up, dorsal to the right. A quantitative analysis of the corresponding data sets is provided in ***Figure 1E and F***. Scalebars: 200 µm.

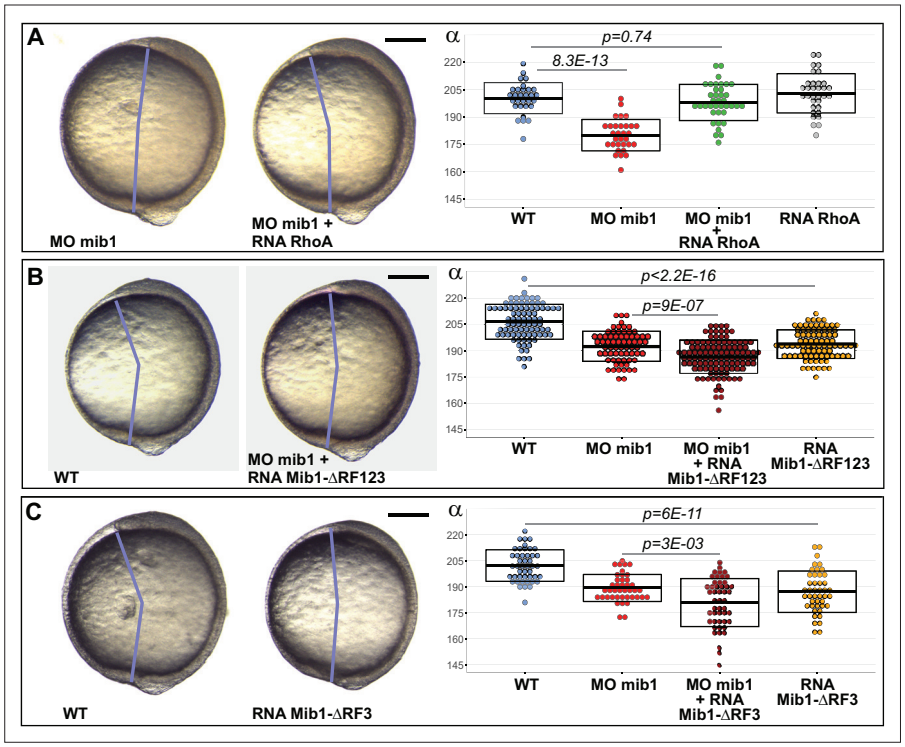

Figure 2. Mib1 controls PCP through its RING finger domains. (**A**) RhoA overexpression rescues mib1 morphant axis extension. (**B,C**) Mib1 proteins lacking all (Mib1ΔRF123, **B**) or only the last (Mib1ΔRF3, **C**) RING finger impair axis extension in mib1 morphant or WT embryos. Lateral views of bud stage embryos, anterior up, dorsal to the right. Scalebars: 200 µm. Boxes represent mean values ± SD. ***Figure 2—source data 1*** for complete statistical information.

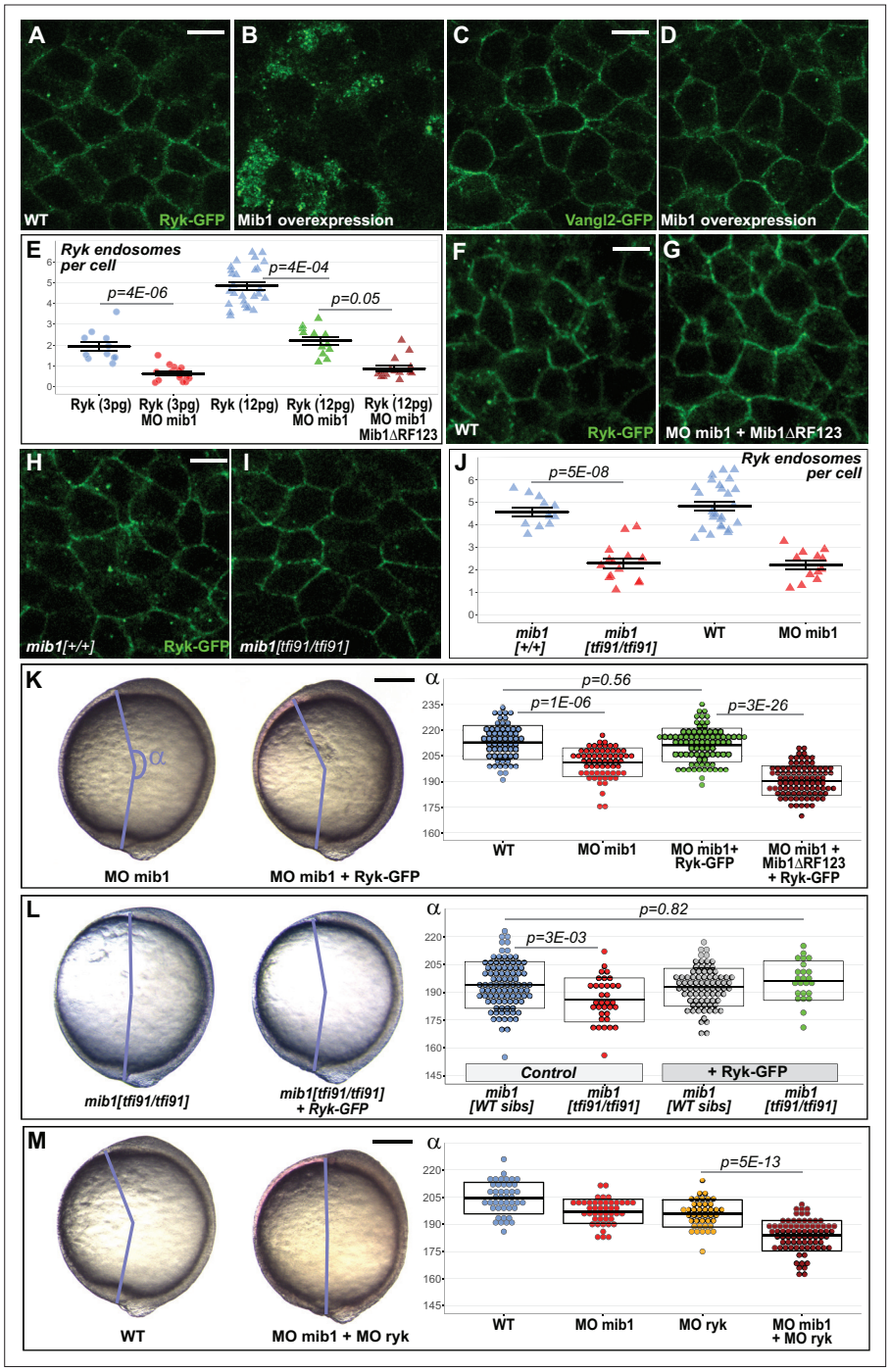

Figure 3. Mib1-mediated Ryk endocytosis controls Convergent Extension movements. (**A–D**) WT mib1 RNA injection triggers Ryk internalization in 20/21 embryos (**B**) but has no effect on Vangl2 localization (D, n = 23). (**E–G**) Mib1 morpholino injection reduces the number of Ryk endosomes that are present upon injection of Ryk-GFP RNA. Increasing the dose of Ryk-GFP RNA restores endosome number in mib1 morphants but not in embryos coinjected with Mib1ΔRF123. (**H–J**) The number of Ryk endosomes that are present upon injection of Ryk-GFP RNA (12 pg) is reduced in mib1 null mutants. mib1 morphant data from panel E are shown again for comparison. (**K**) Ryk-GFP RNA (12 pg) rescues axis extension in mib1 morphants but not in embryos coinjected with Mib1ΔRF123. (**L**) Similarly Ryk-GFP injection rescues axis extension in *mib1*^{tfi91} mutants. (**M**) Ryk morpholino injection aggravates mib1 morphant axis extension phenotypes. (**A–D,F,G,H,I**) dorsal views of 90% epiboly stage embryos, anterior up, scalebars 10 μm. (**K,L,M**) Lateral views of bud stage embryos, anterior up, scalebars 200 μm. In (**E,J**) each data point represents the mean number of endosomes for 20 cells from a single embryo.

Figure 3 continued on next page

Figure 3 continued

For comparison J again includes the mib1 morphant from panel E. Bars represent mean values ± SEM. In (**K,L,M**) boxes represent mean values ± SD. See ***Figure 3—source data 1*** for complete statistical information.

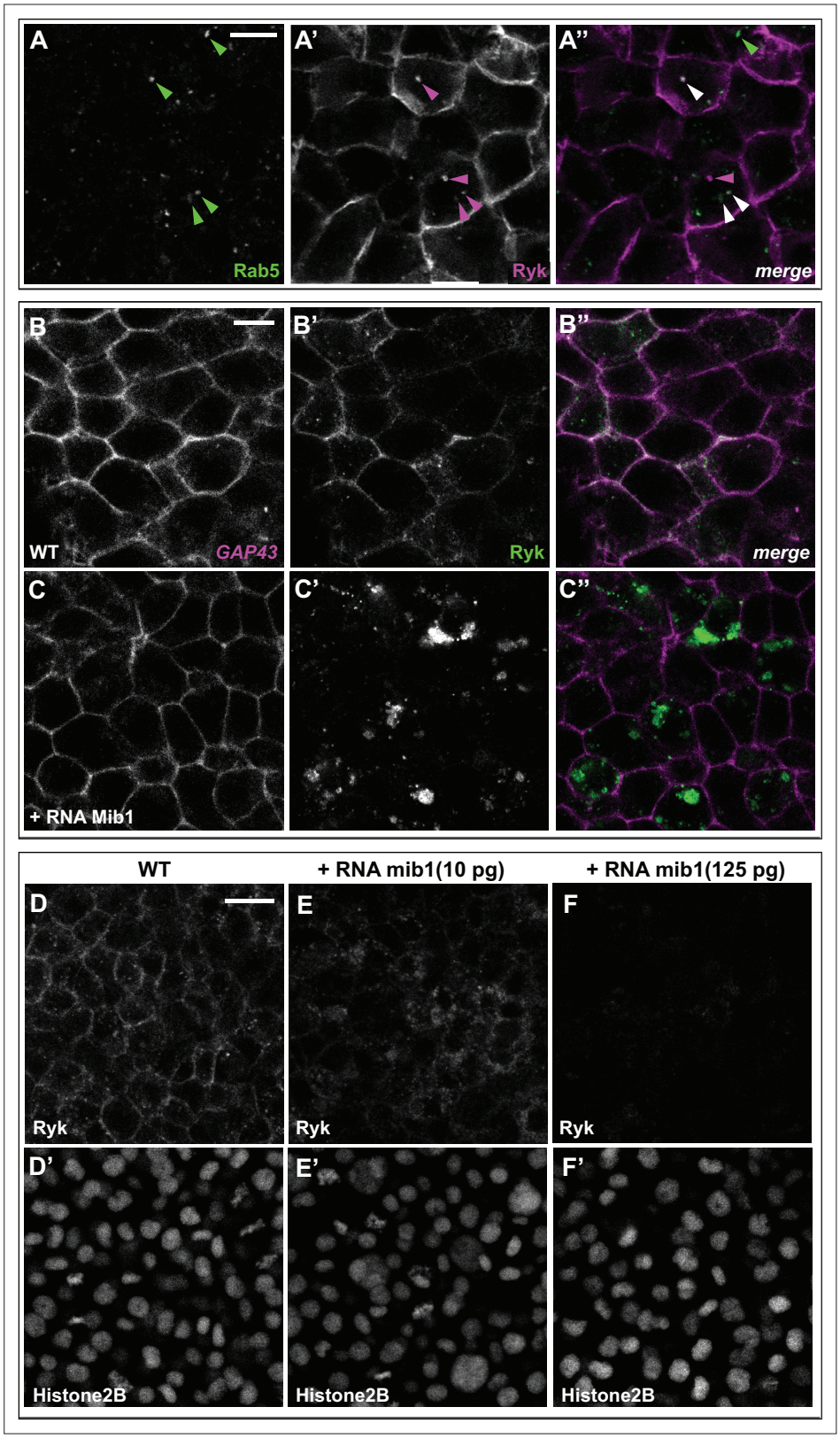

Figure 3—figure supplement 1. Mib1 promotes Ryk internalization and degradation. (**A**) Coinjection of RNAs encoding Rab5-GFP and Flag-Ryk-Myc reveals that 70.7% of Ryk-expressing intracellular compartments are positive for the early endosomal marker Rab5 (n = 75 cells from eight embryos analyzed). Arrowheads in A" indicate compartments that are positive for Rab5 only (green), Ryk only (magenta), or present both markers (white).

Figure 3—figure supplement 1 continued on next page

Figure 3—figure supplement 1 continued

(**B,C**) Mib1 overexpression promotes the internalization of Ryk-GFP but not the one of the plasma membrane marker GAP43-RFP (n = 4). (**D,E**) RNAs encoding Ryk-GFP and Histone2B-mRFP were injected with increasing amounts of mib1 RNA. While a low dose of Mib1 relocalizes Ryk from the plasma membrane to intracellular compartments (n = 6), high amounts of Mib1 cause an overall loss of Ryk signal (n = 6). D'-F', The Histone2B-mRFP signal was used to ascertain that embryos had received a comparable amount of injected material. (**D-F and D'-F'**) are sum projections of three consecutive slices from confocal stacks. All pictures depict dorsal views of 90% epiboly stage embryos, anterior up. Scalebars: 10 µm in A-C, 20 µm in D-F.

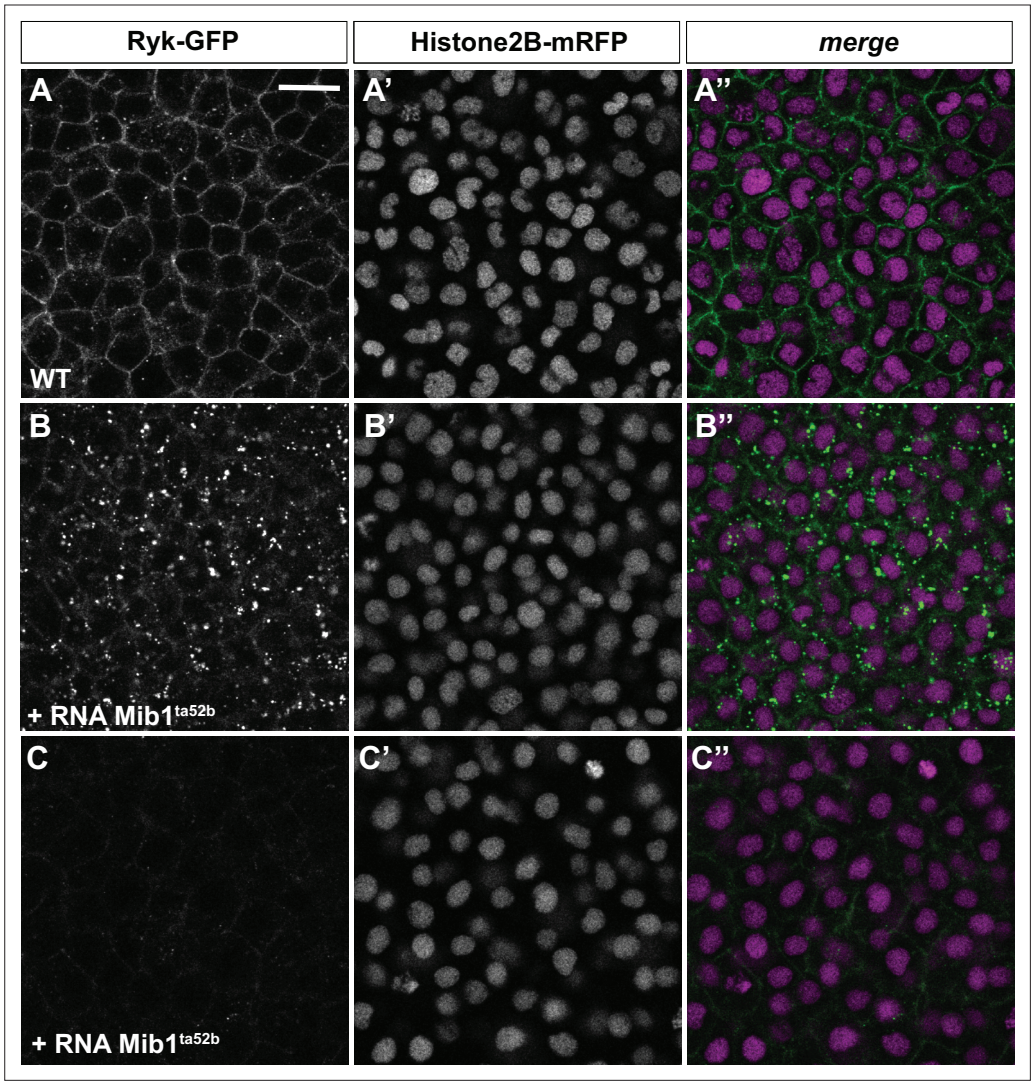

Figure 3—figure supplement 2. Mib1^{ta52b} overexpression promotes Ryk internalization. (**A–C**) Microinjection of RNA encoding the Mib1^{ta52b} mutant protein induces Ryk internalisation (B, n = 16/23 embryos) or degradation (C, n = 7/23 embryos) as compared to WT controls (A, n = 21). Dorsal views of 90% epiboly stage embryos, anterior up. The Histone2B-mRFP signal (**A'-C'**) was used to ascertain that control and Mib1^{ta52b}-expressing embryos had received comparable amounts of injected material. Scalebar: 20 µm.

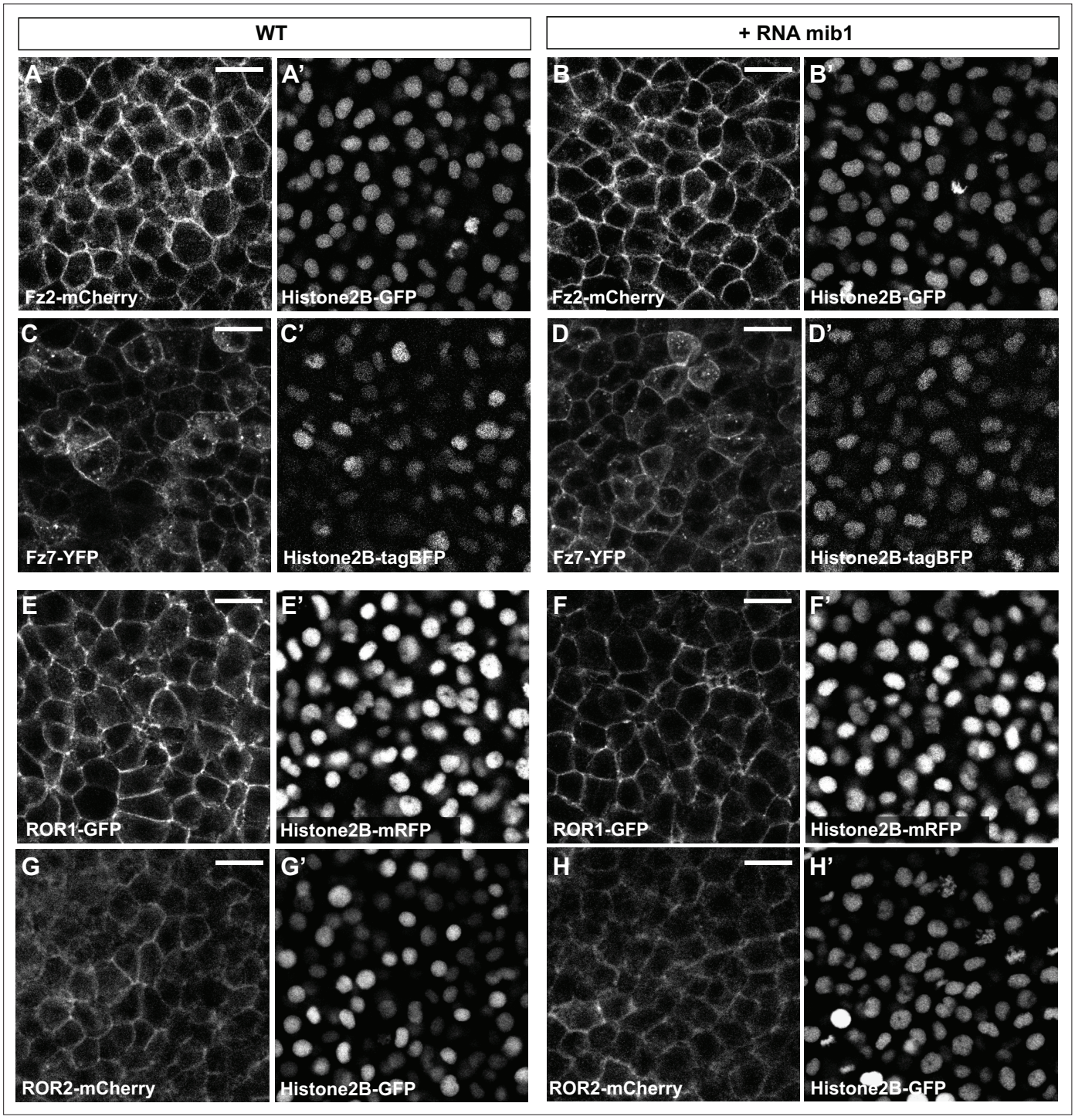

Figure 3—figure supplement 3. Mib1 overexpression does not affect Frizzled/Ror localization. (**A–D**) Mib1 overexpression has no effect on the localization of the Wnt receptors Frizzled2 (Fz2, n = 6) or Frizzled7 (Fz7, n = 8). (**E–H**) Mib1 overexpression has no effect on the localization of the Wnt-binding receptor tyrosine kinases ROR1 (n = 7) or ROR2 (n = 10). All pictures depict dorsal views of 90% epiboly stage embryos, anterior up. (**G,H**) are sum projections of three consecutive confocal slices. A'-H' Display the signal for fluorescently tagged Histone2B constructs that were coinjected to ascertain that control and mib1-expressing embryos had received a comparable amounts of injected material. Scalebars: 20 µm.

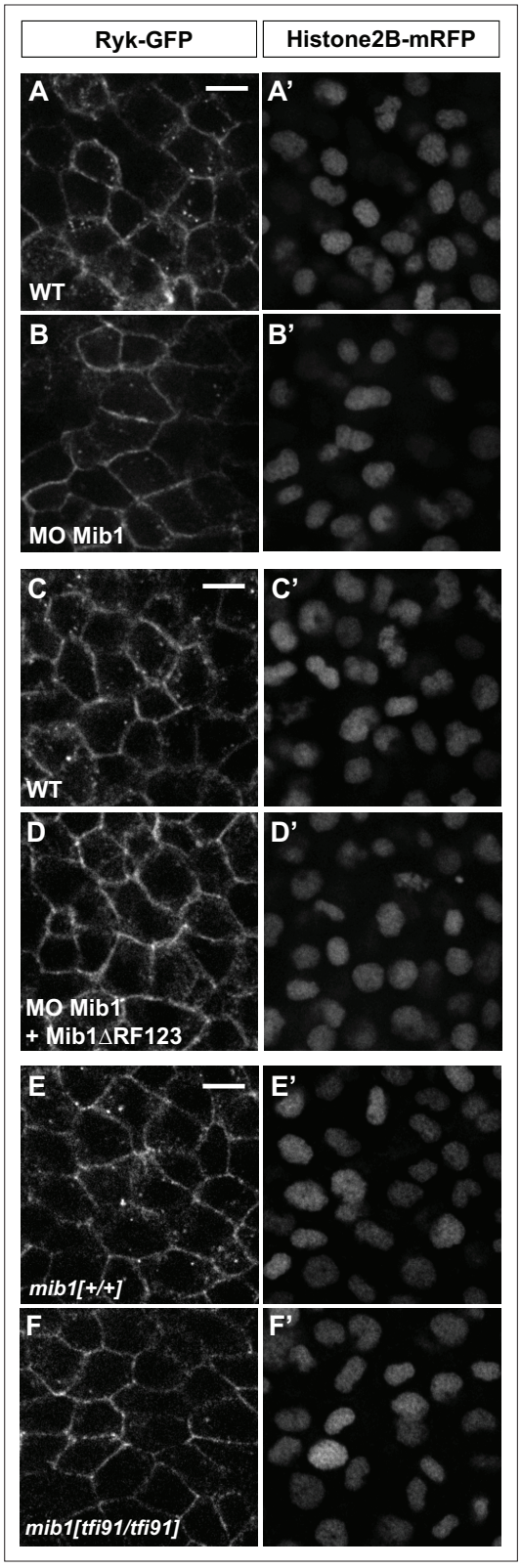

Figure 3—figure supplement 4. Mib1 loss of function impairs Ryk endocytosis. (**A,B**) mib1 morpholino (MO mib1) injection reduces Ryk endocytosis. (**C,D**) A more pronounced inhibition of Ryk endocytosis is observed

Figure 3—figure supplement 4 continued on next page

Figure 3—figure supplement 4 continued

upon coinjection of MO mib1 and RNA encoding dominant-negative Mib1 (mib1DRF123). (**E,F**) Ryk endocytosis is reduced in *mib1*^{tfi91} mutant embryos. All pictures depict dorsal views of 90% epiboly stage embryos, anterior up. A'-F', The Histone2B-mRFP signal was used to ascertain that control and mib1-depleted embryos had received a comparable amount of injected material. Embryos depicted in A-F were injected with 12 pg Ryk-GFP RNA. (**C-F**) correspond to the display items also shown in ***Figure 3F–I***. Scalebars: 10 µm.

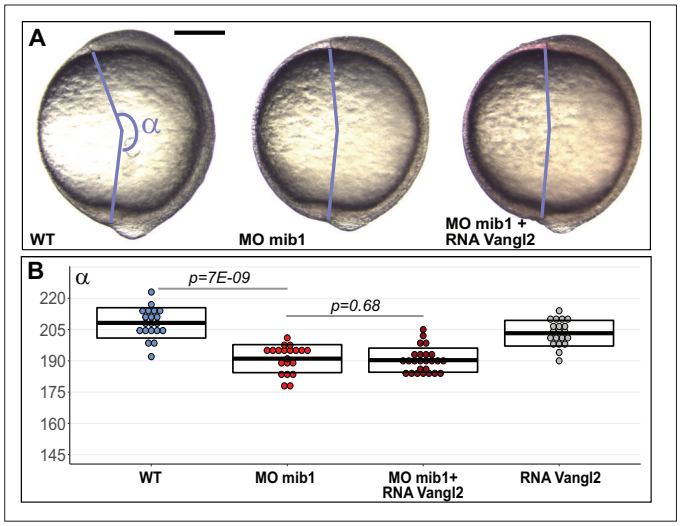

Figure 3—figure supplement 5. mib1 morphant defects are not rescued upon vangl2 overexpression. (**A,B**) vangl2 RNA injection does not rescue axis extension in mib1 morphants. (**A**) Lateral views of bud stage embryos, anterior up, dorsal to the right. Scalebar 200 μm. In (**B**) boxes represent mean values ± SD. See ***Figure 3—source data 1*** for complete statistical information.

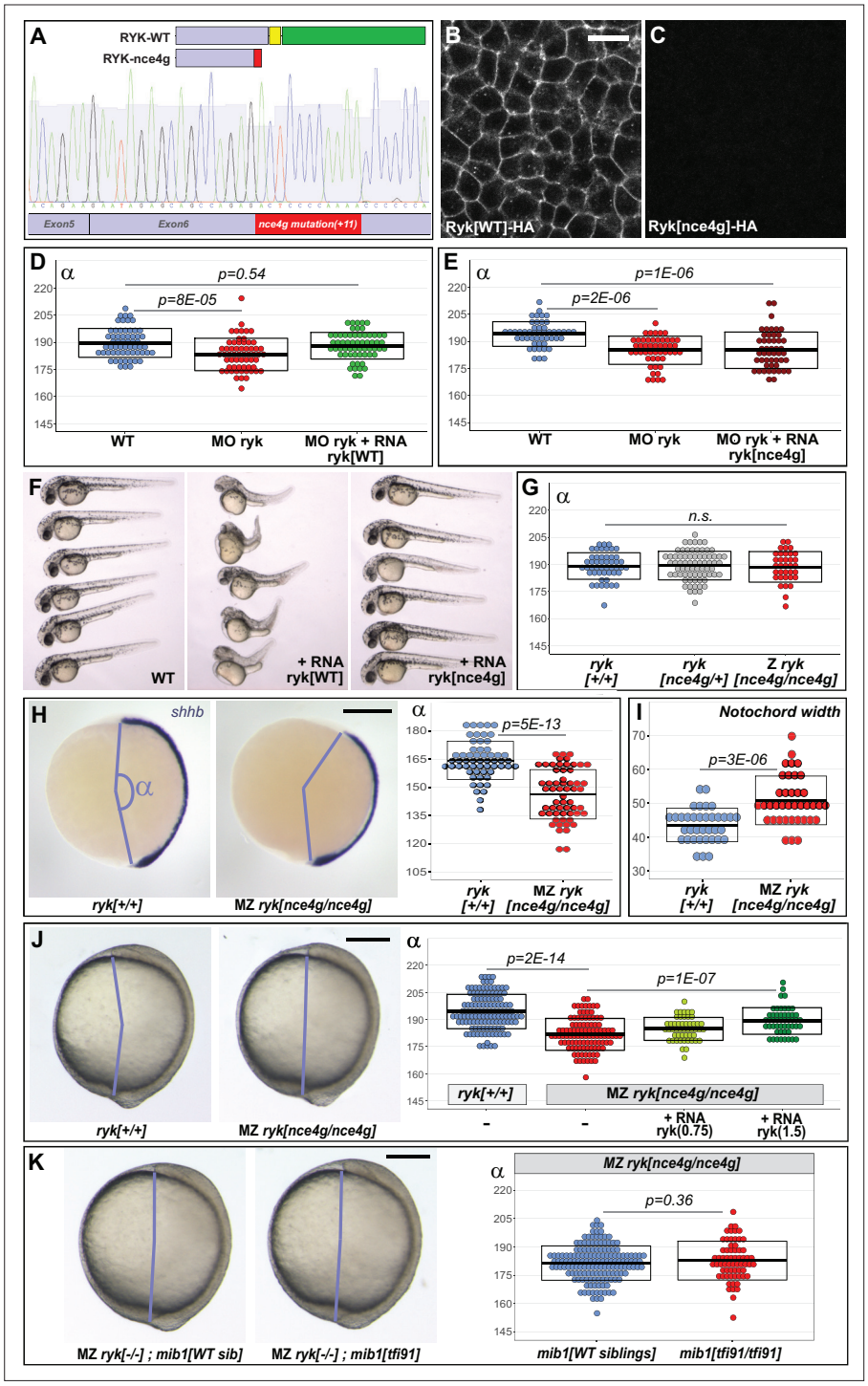

Figure 4. *mib1* loss of function has no effect on convergent extension in maternal zygotic *ryk* mutants. (**A**) *ryk*^{nce4g} mutants present an 11 base pair insertion in exon 6. The RYK-nce4g mutant protein comprises only part of the extracellular (blue) and lacks the entire transmembrane (yellow) and intracellular (green) domains. (**B,C**) Accordingly, a C-terminal HA tag that allows to localize WT Ryk (B, n = 12) becomes undetectable upon introduction of the *ryk*^{nce4g} mutation (C, n = 14). Dorsal views of 90% epiboly stage embryos, anterior up. Scalebar 20 µm. (**D,E**) The Convergent Extension (CE) phenotypes of ryk morphant animals can be rescued using 1.5 pg WT ryk (**D**) but not ryk^{nce4g} mutant (**E**) RNA. (**F**) Overexpressing high levels (25 pg) WT ryk RNA causes severe embryonic malformations while no effect is observed using ryk^{nce4g} mutant RNA. 32 hpf embryos, anterior to the left, dorsal up (n = 24 embryos/condition). (**G**) Zygotic (Z) *ryk* loss of function does not impair CE. (**H–J**) In contrast, Maternal Zygotic (MZ) *ryk* mutants present characteristic CE phenotypes such as a reduced axial elongation (H, *shhb* in situ

Figure 4 continued on next page

Figure 4 continued

hybridization) and an increased width of the notochord (I, *foxa3* in situ hybridization, see also ***Figure 4—figure supplement 1F***). (**J**) ryk WT RNA injection allows a significant rescue of MZ *ryk* mutant CE defects. (**K**) Similar CE defects are observed in MZ *ryk* single mutants and MZ *ryk; mib1* double mutants. (**H,J,K**) Lateral views of bud stage embryos, anterior up, dorsal to the right. Scalebars 200 µm. In (**D,E,G–K**) boxes represent mean values ± SD. See ***Figure 4—source data 1*** for complete statistical information.

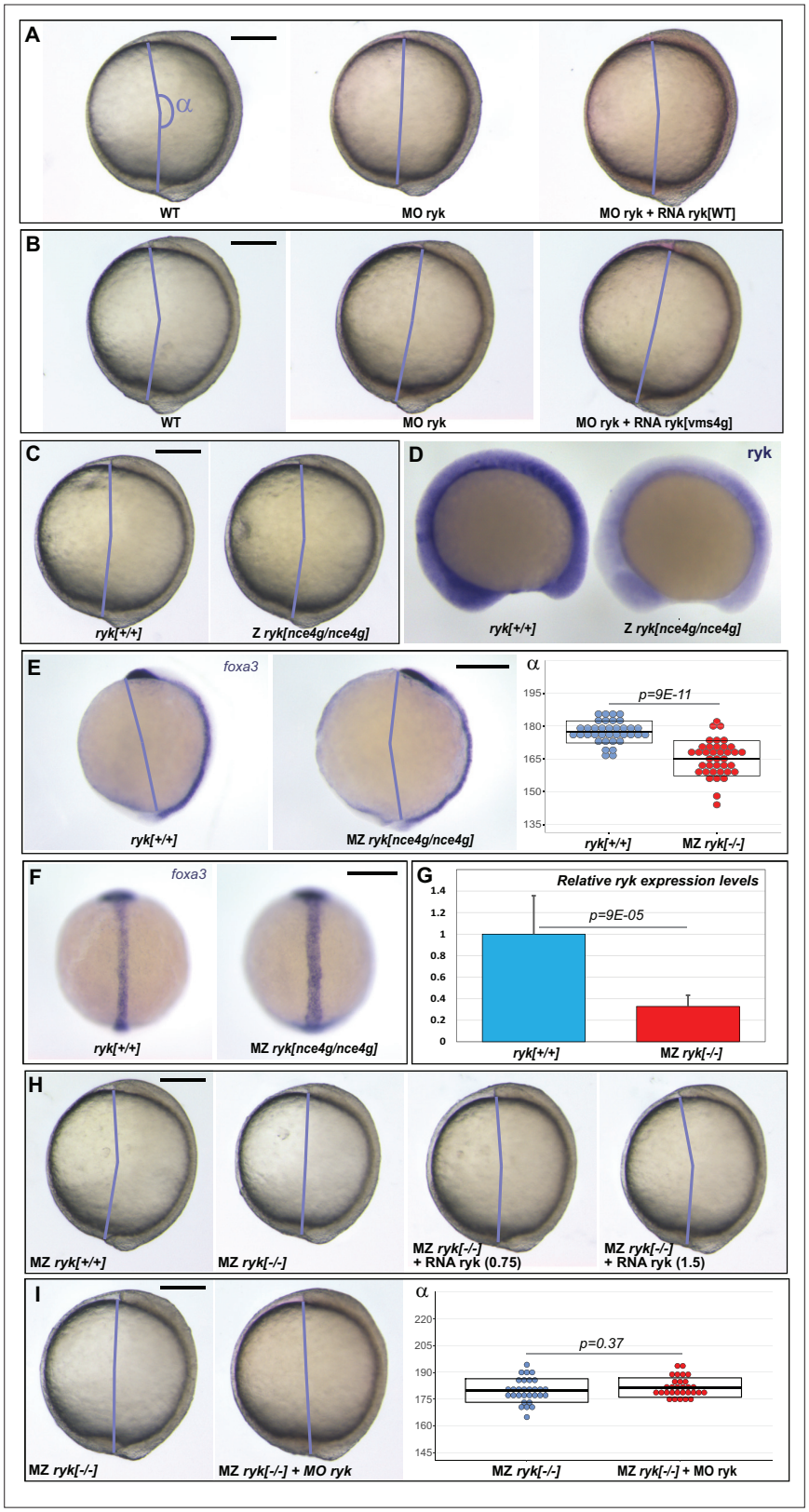

Figure 4—figure supplement 1. Maternal zygotic *ryk*^{nce4g} mutants present Convergent Extension defects. (**A,B**) ryk morphants present Convergent Extension (CE) defects that can be rescued by WT ryk (**A**) but not ryk^{nce4g} mutant (**B**) RNA. (**C**) CE is similar in Zygotic (Z) *ryk*^{nce4g} mutants and their WT siblings. (**D**) In situ hybridization reveals that *ryk* transcript levels are reduced in Z *ryk*^{nce4g} mutants (n = 24) compared to WT siblings (n = 24). 12 somite

Figure 4—figure supplement 1 continued on next page

Figure 4—figure supplement 1 continued

stage embryos, anterior to the left, dorsal up. To warrant identical acquisition conditions, two embryos were photographed on a single picture. (**E–F**) *foxa3* in situ hybridization shows that Maternal Zygotic (MZ) *ryk* mutants present a reduced axial elongation (**E**) and an increased width of the notochord (F, for quantification see ***Figure 4I***). (**G**) qPCR analysis of bud stage embryos reveals that MZ ryk^{nce4g} mutants present reduced *ryk* transcript levels. (**H**) In contrast to Z ryk^{nce4g} mutants, Maternal Zygotic (MZ) ryk^{nce4g} mutants present CE defects. To exclude any defects due to genetic background variation, the parental fish used to obtain the embryos for this experiment were *ryk[+/+]* and *ryk[nce4g/nce4g]* siblings obtained from the same incross. ryk WT RNA injection allows to rescue MZ ryk^{nce4g} mutant CE defects. (**I**) ryk morpholino injection has no effect in MZ ryk^{nce4g} mutants. Lateral (**A,B,C,E,H,I**) or dorsal (**F**) views of bud stage embryos, anterior up. Scalebars 200 µm. Boxes in (**E,I**) boxes represent mean values ± SD. Error bars in **G** represent SE from three biological replicates. Quantitative analysis of the data sets displayed in (**A,B,C,H**) is provided in ***Figure 4D, E, G and H*** respectively. See ***Figure 4—source data 1*** for complete statistical information.

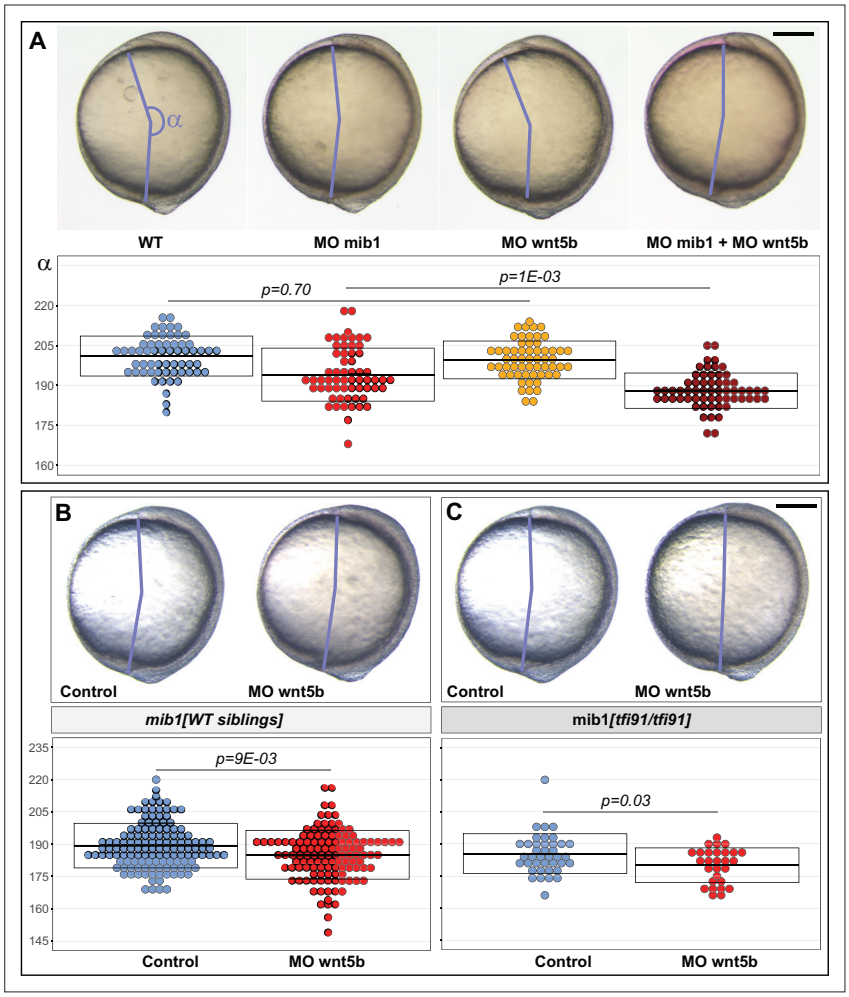

Figure 5. *mib1* interacts with *wnt5b* to control Convergence Extension movements. (**A**) Analysis of the axis extension angle α in bud stage embryos reveals that a subliminal dose of wnt5b morpholino (MO wnt5b) that has no effect on Convergent Extension (CE) in WT significantly enhances the defects observed in animals injected with mib1 morpholino (MO mib1). (**B,C**) wnt5b morpholino injection impairs CE in mib1^{tfi91} WT siblings (**B**) and enhances CE defects in mib1^{tfi91} homozygous mutants (**C**). (**A–C**) Lateral views of bud stage embryos, anterior up, dorsal to the right. Scalebars 200 µm. Boxes represent mean values ± SD. See ***Figure 5—source data 1*** for complete statistical information.

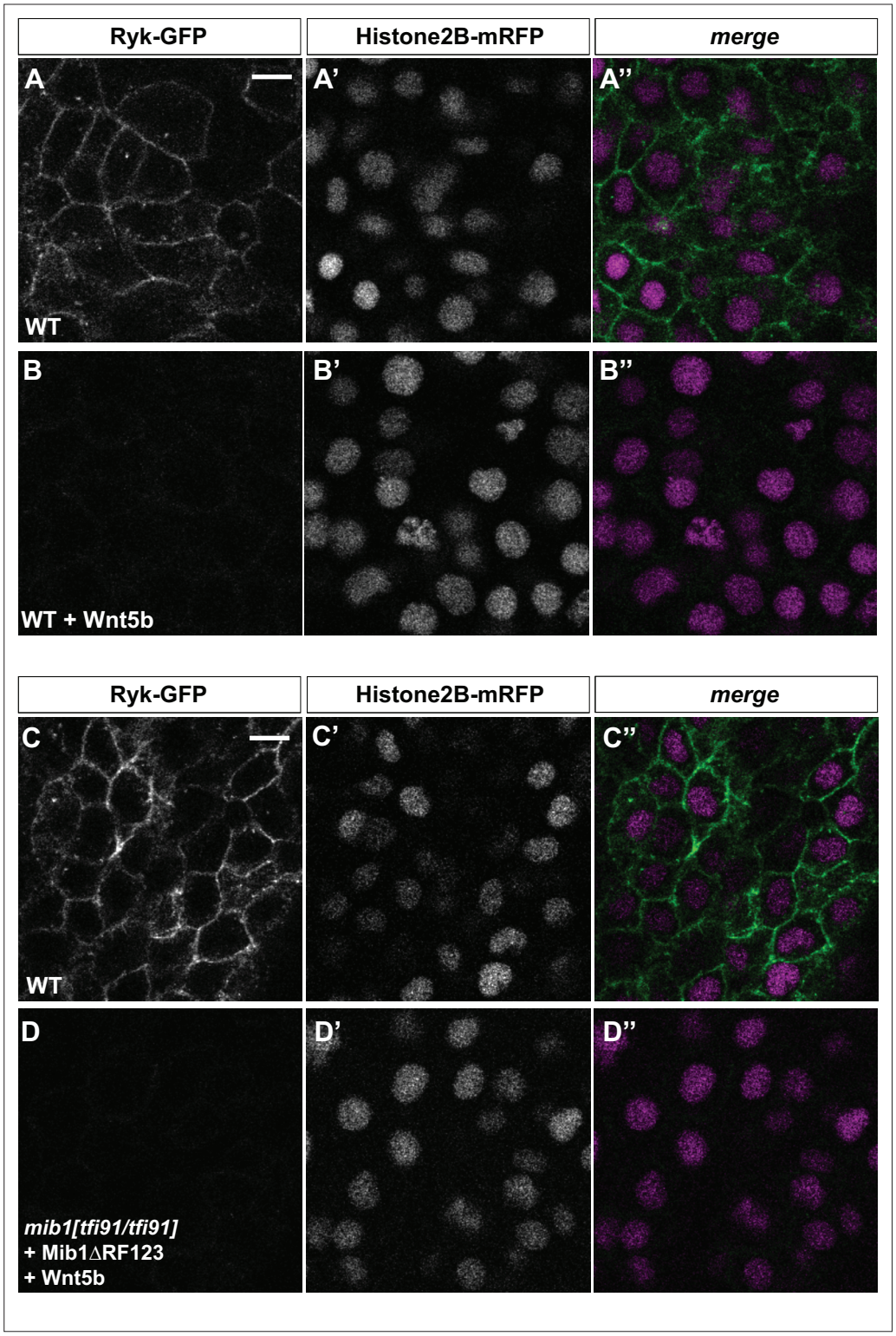

Figure 5—figure supplement 1. Mib1 is dispensable for Wnt5b-induced Ryk degradation. (**A,B**) 17 out of 18 Wnt5b-injected embryos present severely reduced Ryk-GFP signals compared to WT controls (n = 12). (**C,D**) A similar Wnt5b-dependent decrease of Ryk-GFP levels is observed in *mib1*^{tfi91} homozygous mutants that were additionally injected with dominant-negative Mib1ΔRF123 (n = 14 mutant and n = 16 WT control embryos). All pictures depict dorsal views of 90% epiboly stage embryos, anterior up. The Histone2B-mRFP signal (**A'-D'**) was used to ascertain that control and Wnt5b-expressing embryos had received comparable amounts of injected material. Scalebars: 10 µm.